

# The Numerical Computation of Radiation Impedance of Zonal Arrays on a Hard Prolate Spheroidal Baffle

S. HANISH

*Transducer Branch  
Sound Division*

July 27, 1964



**U.S. NAVAL RESEARCH LABORATORY**  
Washington, D.C.



## CONTENTS

Abstract .....	1
Problem Status.....	1
Authorization .....	1
 PART 1 – THE MECHANICAL RADIATION INTERACTION IMPEDANCE BETWEEN ACOUSTIC SOURCES LOCATED IN A PROLATE SPHEROIDAL BAFFLE .....	   1
 PART 2 – THE NUMERICAL COMPUTATION OF ZONAL ARRAYS ON A HARD PROLATE SPHEROIDAL BAFFLE .....	  6
 CONCLUSION .....	 13
 ACKNOWLEDGMENT .....	 13
 REFERENCES.....	 13



# The Numerical Computation of Radiation Impedance of Zonal Arrays on a Hard Prolate Spheroidal Baffle

S. HANISH

*Transducer Branch  
Sound Division*

This report consists of two parts. In the first part the mechanical radiation impedance between "teserai section" sound sources in an acoustically hard prolate spheroidal baffle is analyzed and formulas derived for calculating the impedance in terms of prolate spheroidal wave functions. The particular case of the interaction between zonal sound sources is treated in detail. In the second part a complete numerical study is made of the interaction between eight zones on prolate spheroidal baffle  $2.3\lambda$  long having a radius  $a$  at the equator such that  $ka \approx 3$ . The zones have an axial height of  $\lambda/10$  and are spaced  $\lambda/10$  units apart. Theoretical radiation impedance interaction coefficients are calculated, and tables are presented of mutual and self impedances of all eight zones. Theoretical acoustic beam patterns are calculated and plotted for the condition of equal zonal surface velocities.

---

## PART I — THE MECHANICAL RADIATION INTERACTION IMPEDANCE BETWEEN ACOUSTIC SOURCES LOCATED IN A PROLATE SPHEROIDAL BAFFLE

Two quasi-rectangular rigid pistons ( $i, j$ ) are located on a rigid prolate spheroidal baffle (Fig. 1) whose semifocal distance is  $d/2$ . The spheroidal coordinates  $(\xi, \eta, \phi)$  are related to Cartesian  $(x, y, z)$  coordinates by the coordinate transformation

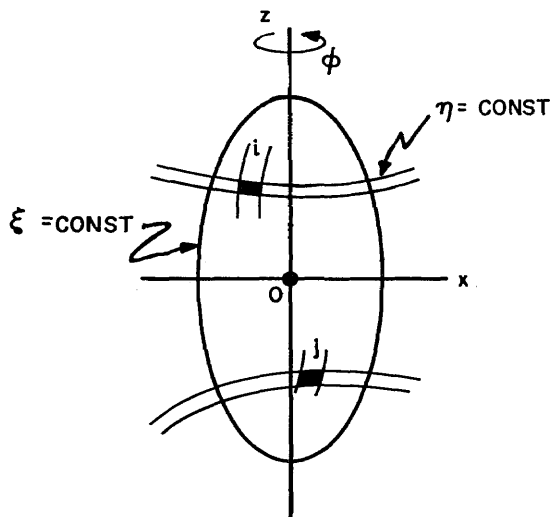


Fig. 1 — Two quasi-rectangular rigid pistons ( $i, j$ ) on a rigid prolate spheroidal baffle

$$\begin{aligned}
x &= \frac{d}{2} \sqrt{(\xi^2 - 1)(1 - \eta^2)} \cos \varphi \\
y &= \frac{d}{2} \sqrt{(\xi^2 - 1)(1 - \eta^2)} \sin \varphi \\
z &= \frac{d}{2} \xi \eta.
\end{aligned} \tag{1}$$

Let  $\Phi_i(\xi, \eta, \varphi, t)$  be the velocity potential of the sound field due to rigid body motion of piston  $i$ . For sinusoidal time variation of frequency  $\omega$  we write

$$\Phi_i(\xi, \eta, \varphi, t) = e^{j\omega t} \psi_i(\xi, \eta, \varphi) \tag{2}$$

in which  $j = \sqrt{-1}$ . The space-dependent velocity potential  $\psi_i$  satisfies the differential equation

$$\nabla^2 \psi_i + k^2 \psi_i = 0, \quad k = \omega/c. \tag{3a}$$

We expand  $\psi_i$  in a doubly infinite series of the spheroidal eigenfunctions corresponding to Eq. (3a):

$$\psi_i(\xi, \eta, \varphi) = \sum_m \sum_n A_{mni} R_{mn}^{(4)}(h, \xi) S_{mn}(h, \eta) \frac{\cos m\varphi}{\sin m\varphi} \tag{3b}$$

in which

$$h = kd/2 \tag{3c}$$

and

$$R_{mn}^{(4)}(h, \xi) = R_{mn}^{(1)}(h, \xi) - jR_{mn}^{(2)}(h, \xi). \tag{3d}$$

The spheroidal radial functions  $R_{mn}^{(1)}$  and  $R_{mn}^{(2)}$  and the spheroidal angle functions  $S_{mn}$  used here are defined by Flammer (1). We locate the  $i$ th piston symmetrically at the origin of the  $\varphi$  coordinate and assign to the  $i$ th piston an azimuthal angular width of  $2\varphi_i$  and a meridional angular width of  $\eta_{i_2} - \eta_{i_1}$ . The velocity  $v(\eta, \varphi)$  of the  $i$ th rigid piston is normal to the surface  $\xi = \xi_0$  and has a magnitude  $u$ ; that is,

$$\begin{aligned}
|v(\eta, \varphi)|_{\xi=\xi_0} &= u, \text{ when } \begin{cases} \eta_{i_1} \leq \eta \leq \eta_{i_2} \\ -\varphi_i \leq \varphi \leq \varphi_i \end{cases} \\
&= 0 \text{ elsewhere.}
\end{aligned} \tag{4}$$

Let  $Q_\xi$  be the scale factor of coordinate  $\xi$ . Then

$$|v(\eta, \varphi)|_{\xi=\xi_0} = \left( \frac{-1}{Q_\xi} \frac{\partial \psi_i}{\partial \xi} \right)_{\xi=\xi_0} \tag{5a}$$

so that

$$[Q_\xi |v(\eta, \varphi)|]_{\xi=\xi_0} = - \sum_m \sum_n A_{mni} \left[ \frac{\partial R_{mn}^{(4)}(h, \xi)}{\partial \xi} \right]_{\xi=\xi_0} S_{mn}(h, \eta) \cos m\varphi \tag{5b}$$

in which

$$Q_\xi = \frac{d}{2} \frac{\sqrt{\xi_o^2 - \eta^2}}{\sqrt{\xi_o^2 - 1}}. \quad (5c)$$

We multiply both sides of Eq. (5b) by  $S_{pq}(h, \eta) \cos p\varphi d\eta d\varphi$  and integrate between the limits  $\eta = +1, -1$  and  $\varphi = 0, \pi$ . If  $p \neq m$  and  $q \neq n$ , the resultant integrals are identically zero. For the case  $p = m$  and  $q = n$ , we find that

$$A_{mni} = \frac{-u \sin m\varphi_i \left(\frac{d}{2}\right) \int_{\eta_{i1}}^{\eta_{i2}} \sqrt{\xi_o^2 - \eta^2} S_{mn}(h, \eta) d\eta}{\epsilon m \left(\frac{\pi}{2}\right) N_{mn} \sqrt{\xi_o^2 - 1} \left[ \frac{\partial R^{(4)}_{mn}(h, \xi)}{\partial \xi} \right]_{\xi=\xi_o}} \quad (6a)$$

in which

$$N_{mn} = \int_{-1}^{+1} [S_{mn}(h, \eta)]^2 d\eta \quad (6b)$$

and

$$\epsilon = 2, m = 0$$

$$\epsilon = 1, m \neq 0.$$

The pressure  $p_i$  of the  $i$ th piston is

$$p_i = j\omega\rho\Psi_i$$

or

$$p_i = \frac{-j\omega\rho 2u \left(\frac{d}{2}\right)}{\pi \sqrt{\xi_o^2 - 1}} \sum_m \sum_n \frac{\sin m\varphi_i \int_{\eta_{i1}}^{\eta_{i2}} \sqrt{\xi_o^2 - \eta^2} S_{mn}(h, \eta) d\eta}{\epsilon m N_{mn} \left[ \frac{\partial R^{(4)}(h, \xi)}{\partial \xi} \right]_{\xi=\xi_o}} \times R^{(4)}_{mn}(h, \xi) S_{mn}(h, \eta) \cos m\varphi. \quad (7)$$

The mechanical force  $F_{ij}$  induced on the area  $A_j$  of the  $j$ th piston by the pressure  $p_i$  is

$$F_{ij} = \int_{A_j} p_i dA_j. \quad (8a)$$

The angular limits of the  $j$ th piston are  $\eta_{j2}, \eta_{j1}$  and  $\varphi_{j2}, \varphi_{j1}$ . We find therefore that

$$F_{ij} = \int_{\eta_{j1}}^{\eta_{j2}} \int_{\varphi_{j1}}^{\varphi_{j2}} p_i(\xi_o, \eta, \varphi) Q_\eta Q_\varphi d\eta d\varphi \quad (8b)$$

in which  $Q_\eta, Q_\varphi$  are scale factors and

$$Q_\eta Q_\varphi = \left( \frac{d}{2} \frac{\sqrt{\xi_o^2 - \eta^2}}{\sqrt{1 - \eta^2}} \right) \left( \frac{d}{2} \sqrt{\xi_o^2 - 1} \sqrt{1 - \eta^2} \right). \quad (8c)$$

Substituting Eqs. (8c) and (7) into Eq. (8b) and integrating with respect to  $\varphi$  we find the interaction mechanical impedance coefficient  $Z_{ij}$  ( $= F_{ij}/u$ ) to be

$$Z_{ij} = \frac{-j2h\rho c \left(\frac{d}{2}\right)^2}{\epsilon\pi} \sum_m \sum_n \frac{\sin m\varphi_i [\sin m\varphi_{j_2} - \sin m\varphi_{j_1}] R_{mn}^{(4)}(h, \xi_o)}{m^2 N_{mn} \left[ \frac{\partial R^{(4)}(h, \xi_o)}{\partial \xi} \right]_{\xi=\xi_o}} \times \int_{\eta_{i_1}}^{\eta_{i_2}} \sqrt{\xi_o^2 - \eta^2} S_{mn}(h, \eta) d\eta \int_{\eta_{j_1}}^{\eta_{j_2}} \sqrt{\xi_o^2 - \eta^2} S_{mn}(h, \eta) d\eta. \quad (9)$$

When  $m \rightarrow 0$  and  $\varphi_i \rightarrow \pi$ ,

$$\lim_{m \rightarrow 0} \frac{\sin m\varphi_i}{\epsilon \left(\frac{\pi}{2}\right) m} \rightarrow 1. \quad (10a)$$

Also when  $m \rightarrow 0$ ,  $\varphi_{j_2} \rightarrow +\pi$  and  $\varphi_{j_1} \rightarrow -\pi$ , so that

$$\lim_{m \rightarrow 0} \frac{\sin m\varphi_{j_2} - \sin m\varphi_{j_1}}{m} = 2\pi. \quad (10b)$$

Therefore when the rigid pistons are replaced by integral rings (that is, when  $m=0$ ) the interaction impedance coefficient between the  $i$ th ring and the  $j$ th ring is

$$Z_{ij} = -j2\pi h\rho c \left(\frac{d}{2}\right)^2 \sum_n \frac{R_{0n}^{(4)}(h, \xi_o)}{N_{0n} \left[ \frac{dR^{(4)}(h, \xi)}{d\xi} \right]_{\xi=\xi_o}} \int_{\eta_{i_1}}^{\eta_{i_2}} \sqrt{\xi_o^2 - \eta^2} S_{0n}(h, \eta) d\eta \times \int_{\eta_{j_1}}^{\eta_{j_2}} \sqrt{\xi_o^2 - \eta^2} S_{0n}(h, \eta) d\eta. \quad (11)$$

If the (complex) velocities of the  $i$ th and  $j$ th pistons are  $V_i e^{j\delta_i}$ ,  $V_j e^{j\delta_j}$  respectively, the interaction impedance  $z_{ij}$  is found by multiplying the impedance coefficient  $Z_{ij}$  referred to  $V_i$  by the ratio of velocities; that is

$$z_{ij} = Z_{ij} \frac{V_j}{V_i} e^{j(\delta_j - \delta_i)}. \quad (12)$$

In some piston arrays, the velocity  $V$  normal to the  $z$ -axis rather than the velocity  $v$  normal to the spheroidal surface is fixed. Let  $\alpha$  be the angle between the two normals at any point on the ellipsoidal surface. Then for piston  $i$  we have

$$[v(\eta, \varphi)]_{\xi=\xi_o} = -V_i |\cos \alpha|, \text{ when } \begin{cases} \eta_{i_1} \leq \eta \leq \eta_{i_2} \\ -\varphi_i \leq \varphi \leq \varphi_i \end{cases} \quad (13)$$

$= 0$  elsewhere.

Let

$$r = \sqrt{x^2 + y^2} = \frac{d}{2} \sqrt{(\xi^2 - 1)(1 - \eta^2)}. \quad (14a)$$

If the normal to the surface is  $N$ , then

$$|\cos \alpha| = \frac{\partial r}{\partial N} = \frac{d}{2} \frac{\xi \sqrt{1 - \eta^2}}{Q_\xi \sqrt{\xi^2 - 1}}. \quad (14b)$$

We equate the normal component of velocity  $\partial \Psi / \partial N$  with the value of the velocity given by Eq. (13) and find

$$\frac{-V_i \left( \frac{d}{2} \right) \xi_o \sqrt{1 - \eta^2}}{\sqrt{\xi_o^2 - 1}} = \sum_m \sum_n A_{mni} \left[ \frac{dR_{mn}^{(4)}(h, \xi)}{d\xi} \right]_{\xi=\xi_o} S_{mn}(h, \eta) \cos m\varphi. \quad (15)$$

Multiplying both sides of Eq. (15) by  $S_{pq}(h, \eta) \cos q\varphi d\eta d\varphi$  and integrating  $\eta$  between  $+1$  and  $-1$  and  $\varphi$  between  $0$  and  $\pi$ , we find that

$$A_{mni} = \frac{-V_i \left( \frac{d}{2} \right) \xi_o \sin m\varphi_i \int_{\eta_{i1}}^{\eta_{i2}} \sqrt{1 - \eta^2} S_{mn}(h, \eta) d\eta}{\epsilon N_{mn} \left( \frac{\pi}{2} \right) \left[ \frac{dR_{mn}^{(4)}(h, \xi)}{d\xi} \right]_{\xi=\xi_o} m \sqrt{\xi_o^2 - 1}}. \quad (16a)$$

The pressure  $p_i$  is therefore

$$p_i(\xi, \eta, \varphi) = \frac{j\omega\rho V_i \left( \frac{d}{2} \right) \xi_o}{\epsilon \left( \frac{\pi}{2} \right) \sqrt{\xi_o^2 - 1}} \sum_m \sum_n \frac{\sin m\varphi_i \int_{\eta_{i1}}^{\eta_{i2}} \sqrt{1 - \eta^2} S_{mn}(h, \eta) d\eta}{m N_{mn} \left[ \frac{dR_{mn}^{(4)}(h, \xi)}{d\xi} \right]_{\xi=\xi_o}} \times R_{mn}^{(4)}(h, \xi) S_{mn}(h, \eta) \cos m\varphi. \quad (16b)$$

The z-component of interaction force  $(F_{ij})_z$  induced over the area  $A_j$  of the  $j$ th piston by the  $i$ th piston is found to be

$$(F_{ij})_z = \int p_i |\cos \alpha| dA_j \quad (17a)$$

$$= \iint p_i |\cos \alpha| (Q_\eta Q_\varphi)_{\xi=\xi_o} d\eta d\varphi \quad (17b)$$

in which the scale-factors  $Q_\eta$ ,  $Q_\varphi$  are computed from

$$Q_\eta = \frac{d}{2} \frac{\sqrt{\xi^2 - \eta^2}}{\sqrt{1 - \eta^2}} \quad (17c)$$

$$Q_\varphi = \frac{d}{2} \sqrt{\xi^2 - 1} \sqrt{1 - \eta^2}. \quad (17d)$$

Inserting Eqs. (5c), (17c), (17d), and (14b) into Eq. (17b), we find

$$(F_{ij})_z = \left(\frac{d}{2}\right)^2 \xi_o \sqrt{\xi_o^2 - 1} \int_{\eta_{j_1}}^{\eta_{j_2}} \int_{\varphi_{j_1}}^{\varphi_{j_2}} p_i(\xi_o, \eta, \varphi) \sqrt{1 - \eta^2} d\eta d\varphi. \quad (17e)$$

By performing the indicated integrations we arrive at mutual interaction impedance coefficient  $Z_{ij}$ .

$$\begin{aligned} Z_{ij} &= \frac{(F_{ij})_z}{|V_i|} \\ &= \frac{-j\omega\rho\left(\frac{d}{2}\right)^3 \xi_o^2}{\epsilon\left(\frac{\pi}{2}\right)} \sum_m \sum_n \frac{\sin m\varphi_i (\sin m\varphi_{j_2} - \sin m\varphi_{j_1})}{m^2 N_{mn}} \\ &\quad \times \frac{R_{mn}^{(4)}(h, \xi_o)}{\left[\frac{dR_{mn}^{(4)}(h, \xi)}{d\xi}\right]_{\xi=\xi_o}} \int_{\eta_{i_1}}^{\eta_{i_2}} \sqrt{1 - \eta^2} S_{mn}(h, \eta) d\eta \int_{\eta_{j_1}}^{\eta_{j_2}} \sqrt{1 - \eta^2} S_{mn}(h, \eta) d\eta. \end{aligned} \quad (18)$$

When  $m \rightarrow 0$  the conditions described by Eqs. (10a) and (10b) hold. The interaction mechanical impedance is no longer the impedance between pistons but the impedance between rings. The impedance coefficient between rings then reduces to

$$\begin{aligned} Z_{ij} &= -j2\pi\left(\frac{kd}{2}\right)\rho c\left(\frac{d}{2}\right)^2 \xi_o^2 \sum_n \frac{R_{0n}^{(4)}(h, \xi_o)}{N_{0n} \left[\frac{dR_{0n}^{(4)}(h, \xi)}{d\xi}\right]_{\xi=\xi_o}} \\ &\quad \times \int_{\eta_{i_1}}^{\eta_{i_2}} \sqrt{1 - \eta^2} S_{0n}(h, \eta) d\eta \int_{\eta_{j_1}}^{\eta_{j_2}} \sqrt{1 - \eta^2} S_{0n}(h, \eta) d\eta. \end{aligned} \quad (19)$$

## PART 2 – THE NUMERICAL COMPUTATION OF ZONAL ARRAYS ON A HARD PROLATE SPHEROIDAL BAFFLE

In Eq. (19) we may write

$$2\pi\left(\frac{kd}{2}\right)\left(\frac{d}{2}\right)^2 \xi_o^2 = \frac{A}{\alpha_i} = A_i \quad (20)$$

where

$A$  = zonal reference area (same for each zone)  
 $\alpha_i$  = constant associated with zone  $i$ .

If we assume the normal component of velocity  $V$  of the  $j$ th zone to be equal in magnitude and phase to the normal component of velocity  $V$  of the  $i$ th zone, then the interaction mechanical impedance coefficient  $Z_{ij}$  between the  $i$ th zone and the  $j$ th zone of Eq. (19) reduces to

$$Z_{ij} = -j\rho c \frac{A}{\alpha_i} \sum_{n=0}^{\infty} \frac{R_{0n}^{(4)}(h, \xi_o)}{N_{0n} \left[\frac{dR_{0n}^{(4)}}{d\xi}\right]_{\xi=\xi_o}} I_i^{0n} I_j^{0n} \quad (21a)$$

$$I_i^{0n} = \int_{\vartheta_i}^{\vartheta_i + \Delta\vartheta_i} S_{0n}(h, \cos \vartheta) \sin^2 \vartheta d\vartheta. \quad (21b)$$

We consider now an array of eight coaxial ring zones symmetrically spaced about the equator on a prolate spheroidal baffle  $2.31\lambda$  long. Each ring is approximately  $0.1\lambda$  in axial length and has a maximum radius  $a$  such as  $ka \approx 3$ . More precisely if  $2L$  is the length of spheroid defined by  $\psi_o = \text{const.}$  with focal distance  $d/2$ , and if the height of each zone is  $\Delta z$  then (see Fig. 1) we require that

$$\begin{aligned} \cosh \psi_o &= 1.100000 & \Delta z &= 0.095\lambda \\ h = \frac{kd}{2} &= 6.600000 & 2L &= 2.311\lambda \\ ka &= 3.024 & k\Delta z &= 0.6. \\ \frac{d}{2} &= 1.050\lambda \end{aligned} \quad (22)$$

In constructing the mathematical model of the array we divided the spheroid into 15 ring zones, seven of which were considered hard baffle (i.e., passive) and the remaining eight vibrating in the breathing mode (i.e., active). The zone at the equator (passive) was numbered 1 and the first active zones above and below the equator were numbered 2, 3 respectively, and so forth. The extent of each zone is defined by two angles  $\vartheta_1, \vartheta_2$  which are selected in accordance with the requirements of Eq. (22). A list of all active zones and their angle limits (in radians) is given in Table 1. Figure 2 shows the zones and spheroidal baffle drawn approximately to scale.

TABLE 1  
Definition of the Active Zones

ith Zone	$\vartheta_2$ (radians)	$\vartheta_1$ (radians)
14	1.003691	0.902261
10	1.189738	1.098931
6	1.362684	1.277345
2	1.529462	1.446508
3	1.695085	1.612131
7	1.864247	1.778909
11	2.042662	1.951855
15	2.239332	2.137902

We begin our calculations with Eq. (21b). The integrand of  $I_t^n$  contains the spheroidal angle function  $S_{0n}(h, \cos \vartheta)$  which is defined in terms of an infinite series of products of Legendre polynomials  $P_r(\cos \vartheta)$  and spheroidal wave expansion constants  $d_r(h/0n)$ ,

$$S_{0n}(h, \cos \vartheta) = \sum_{r=0,1}^{\infty} d_r(h|0n) P_r(\cos \vartheta) \quad (23a)$$

so that

$$I_t^{0n} = \sum_{r=0,1}^{\infty} d_r(h|0n) \int_{\vartheta_1}^{\vartheta_2} P_r(\cos \vartheta) \sin^2 \vartheta d\vartheta. \quad (23b)$$

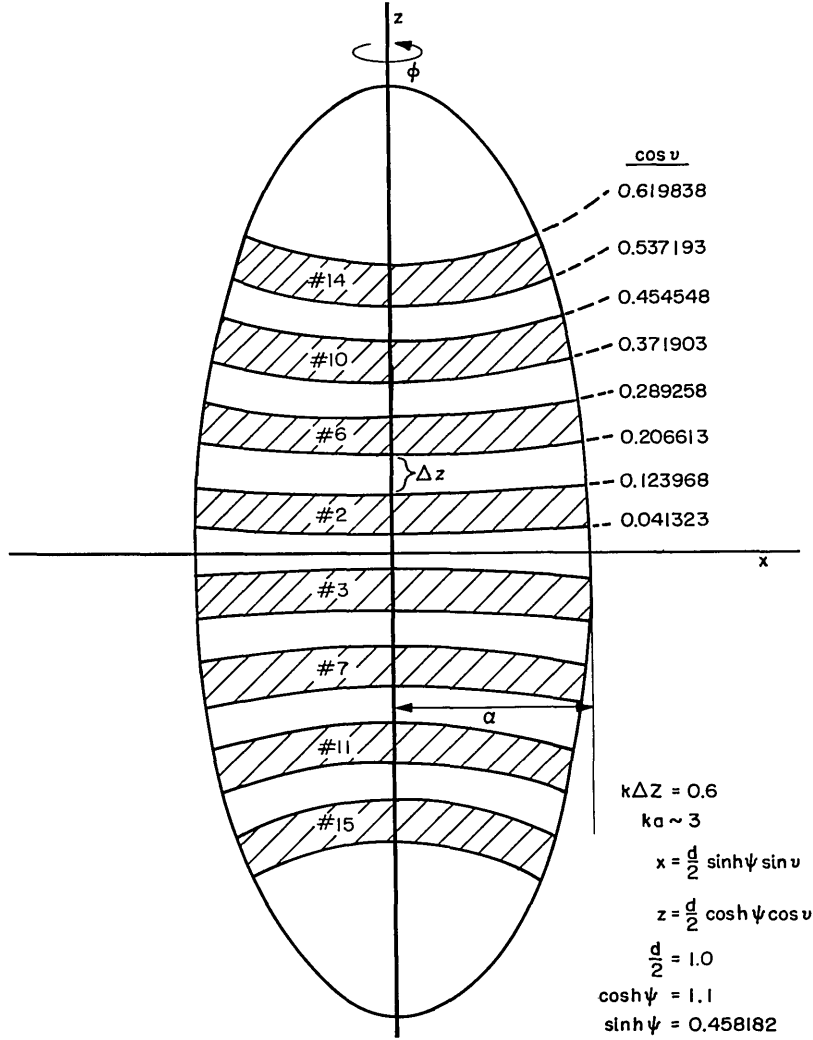


Fig. 2 — The eight active zones drawn to scale on an (acoustically) hard prolate spheroidal baffle

The prime over the summation symbol indicates that  $r$  may be an even integer only, if  $n$  is even, and an odd integer only, if  $n$  is odd. The constants  $d_r(6.6/0n)$  are listed in the tables of Stratton, Morse et al. (2) for  $0 \leq n \leq 8$ . Our calculations however require  $0 \leq n \leq 19$ . To obtain the wave expansion constants corresponding to these values of  $n$  we undertook an extensive program for the calculation of the eigenvalues (to 12 significant digits) associated with the wave equation in spheroidal coordinates. Use of these eigenvalues in a three-term recursion formula in  $d_r(h/0n)$  (see Ref. 1) served to give numerical ratios of the expansion constants also to 12 significant figures. Unique values of  $d_r$  were finally obtained by adoption of a suitable normalization (*i.e.*, that found in Morse and Feshbach (3)). When all the necessary constants had been calculated, the integral in Eq. (23b) was programmed for digital computation on the NAREC computer with limits of integration determined from Table 1 above.

We then calculated the radial spheroidal wave functions  $R_{0n}^{(4)}(h, \xi_0)$  by means of the formula

$$R_{0n}^{(4)}(h, \xi) = R_{0n}^{(1)}(h, \xi_0) - jR_{0n}^{(2)}(h, \xi_0). \quad (24a)$$

The first term on the right is the radial spheroidal wave function of the first type. It may be expanded as a sum of spherical Bessel function  $j_r(h\xi_o)$  multiplied by the spheroidal wave expansion constants noted in Eq. (23a). One has

$$R_{0n}^{(1)}(h, \xi_o) = \sum_{r=0,1}^{\infty} (-j)^{r-n} d_r(h|0n) j_r(h\xi_o). \quad (24b)$$

The second term on the right of Eq. (24a) is the radial spheroidal wave function of the second type. It may be expanded as a sum of associated Legendre functions multiplied by spheroidal wave expansion constants of special type. One has

$$R_{0n}^{(2)}(h, \xi_o) = \frac{1}{K_{mn}^{(2)}(h)} \left[ \sum_{r=-2m, -2m+1}^{\infty} d_r(h|0n) Q_{m+r}^m(\xi_o) + \sum_{r=2m+2, 2m+1}^{\infty} d_{r|p}(h|0n) P_{r-m-1}^m(\xi_o) \right]. \quad (24c)$$

Here  $K_{mn}^{(2)}(h)$  and  $d_{r|p}(h|0n)$  are special factors which are defined and explained by Flammer (1) on pages 27 and 33 respectively. In our calculation we computed  $R_{0n}^{(1)}$  and  $R_{0n}^{(2)}$  with their derivatives and then formed the calculated Wronskian ( $= 1/h(\xi_o^2 - 1)$ ). Comparison with the theoretical Wronskian then gave a measure of the precision achieved. Table 2 shows all of the radial functions actually calculated and used in our problem.

Numerical calculation of the normalization factor  $N_{0n}$  was carried out using the scheme of Morse and Feshbach (3), in which

$$N_{0n} = \sum_{r=0,1}^{\infty} [d_r(h|0n)]^2 \left( \frac{2}{2r+1} \right). \quad (25)$$

This is a rapidly converging series for  $r \approx 50$ .

With the final calculation of  $N_{0n}$  all pertinent factors appearing in Eq. (21a) were available in numerical form. The coefficients of self and mutual interaction impedance  $Z_{ij}$  (read "ith zone acting on jth zone") were then computed to five significant digits for each of the eight rings. Table 3 lists all of these coefficients. We note that the mutual impedance coefficients ( $i \neq j$ ) are appreciable fractions of the self impedance coefficients ( $i = j$ ) and that they may have negative real parts and negative imaginary parts. In Eq. (21a)  $n$  was summed from 0 to 19. The real part converged very rapidly ( $n \approx 6$ ). The imaginary part in contrast converged so slowly that in the author's opinion the entries in Table 3 under "Imaginary" are somewhat in error, perhaps as much as  $\pm 8\%$ . For comparison purposes we note below the self radiation impedance of a ring equivalent to zone 2, located in an infinite cylindrical (hard) baffle. The applicable formulas are found in Robey (4):

$$Z_{22} = \rho c A_2 [0.24398 + j 0.30788], \text{ prolate spheroid}$$

$$Z_{22} = \rho c A_2 [0.24780 + j 0.40198], \text{ infinite cylinder.}$$

The total mechanical impedance on each zone for equal velocity distribution throughout the array was found by summing all impedances on a zone, i.e.,

$$Z_j = \sum_i Z_{ij}.$$

TABLE 2  
Calculated Radial Functions for  $h = 6.6$  and  $\xi_0 = 1.1$

$n$	$R_{0n}^{(1)}$	$A^*$	$R_{0n}^{(2)}$	$A^*$	$R_{0n}^{(1)'}$	$A^*$	$R_{0n}^{(2)'}$	$A^*$	Calculated Wronskian†
0	-0.8394469	-1	0.2025905	0	-0.27805589	1	-0.18844049	1	0.721500722
1	0.2149589	-1	0.2350539	0	-0.31141422	1	-0.4880214	0	0.721500869
2	0.1555883	0	0.2056134	0	-0.27848106	1	0.9570535	0	0.7215007206
3	0.2767677	0	0.7202851	-1	-0.17515040	1	0.2151055	1	0.7215007197
4	0.2887213	0	-0.1491417	0	-0.3604599	0	0.26851512	1	0.7215007184
5	0.18672248	0	-0.3502638	0	0.45719243	0	0.30064016	1	0.72150071735
6	0.8635994	-1	-0.5645129	0	0.4985796	0	0.5095488	1	0.7215007146
7	0.3254378	-1	-0.1051246	1	0.2874713	0	0.1288411	2	0.721500712
8	0.1055804	-1	-0.2490787	1	0.12325483	0	0.3925912	2	0.721500706
9	0.3020672	-2	-0.7193551	1	0.4336670	-1	0.1355791	3	0.7215007002
10	0.7739809	-3	-0.2417554	2	0.1310299	-1	0.5229186	3	0.7215009359
11	0.17970027	-3	-0.9193431	2	0.34906099	-2	0.2229234	4	0.7215008424
12	0.3816147	-4	-0.3887662	3	0.8343541	-3	0.10406635	5	0.7215006457
13	0.7469530	-5	-0.1805984	4	0.18121967	-3	0.5277719	5	0.7215006207
14	0.1356266	-5	-0.9131289	4	0.3611265	-4	0.2888412	6	0.72150056
15	0.2296938	-6	-0.4988129	5	0.6653477	-5	0.1696243	7	0.7215005093
16	0.3645410	-7	-0.2926134	6	0.1140531	-5	0.1063710	8	0.7215003861
17	0.5443908	-8	-0.1833930	7	0.1828632	-6	0.70931009	8	0.7215002836
18	0.7677197	-9	-0.1222656	8	0.2754616	-7	0.5011010	9	0.7215000361
19	0.1025661	-9	-0.8637945	8	0.3913838	-8	0.3738318	10	0.72149983

\*Exponents of 10.

†The theoretical Wronskian is 0.7215007215.

Table 4 lists the total impedances for the eight zones and (for comparison) the corresponding self impedances. We note that the interaction effects increase the radiation resistance by a factor of approximately 2 for most rings and diminish the radiation reactance from 40% to 90% of their self reactance values.

Total impedances of active zones for the case where fewer than eight rings are in the spheroidal baffle have also been calculated. Table 5 lists the total radiation impedances when only two, three, or four zones respectively are in the baffle.

The final set of calculations consisted in determining the variation of pressure amplitude with angle in the far field (*i.e.*, the far-field pressure pattern). We employed here Eq. (16b). Setting  $m = 0$  and using Ref. 2 to write

$$\lim_{h\xi \rightarrow \infty} R_{0n}^{(4)}(h, \xi) \rightarrow (-j)^{-n-1} \frac{e^{-jkr}}{kr}$$

we sum all the zonal pressures  $p_i$  from  $i = 1$  to  $i = 8$ . In general the magnitude and phase of velocity will be different for each zone. Hence we replace  $V_i$  by  $V_i e^{j\delta_i}$  in our sum. Using Eq. (21b) we found the pressure in the far field to be

TABLE 3  
Mutual Impedance Coefficients  $Z_{ij}$

ZONE $i$	ZONE $j$					
	ZONE 14		ZONE 10		ZONE 6	
	Real	Imaginary	Real	Imaginary	Real	Imaginary
14	0.22904	0.30244	0.14967	-0.034830	0.011451	-0.082616
10	0.16310	-0.037956	0.23336	0.30683	0.16066	-0.025709
6	0.013120	-0.094653	0.16890	-0.027029	0.24371	0.30871
2	-0.074086	-0.049525	0.021453	-0.097037	0.17317	-0.024969
3	-0.046074	0.055893	-0.070474	-0.055502	0.020245	-0.099214
7	0.022587	0.037759	-0.049434	0.054730	-0.071888	-0.054004
11	0.040319	0.0029121	0.016910	0.034661	-0.047027	0.052057
15	0.0041070	-0.033709	0.036998	0.0026738	0.019712	0.032957
	ZONE 2		ZONE 3		ZONE 7	
14	-0.063178	-0.042233	-0.039291	0.047663	0.019714	0.032957
10	0.019937	-0.090177	-0.065492	-0.051578	-0.047021	0.052058
6	0.169150	-0.024395	0.019780	-0.096933	-0.071888	-0.054004
2	0.24398	0.30788	0.16909	-0.022733	0.020247	-0.099215
3	0.16909	-0.022733	0.24398	0.30788	0.17313	-0.024968
7	0.019781	-0.096933	0.16915	-0.024394	0.24369	0.30870
11	-0.065492	-0.051579	0.019937	-0.090176	0.16065	-0.025711
15	-0.039291	0.047663	-0.063178	-0.042233	0.011447	-0.082617
	ZONE 11		ZONE 15			
14	0.036998	0.026722	0.0041070	-0.033709		
10	0.016910	0.034661	0.040319	0.0029138		
6	-0.04944	0.054729	0.022584	0.037758		
2	-0.070474	-0.055503	-0.046074	0.055893		
3	0.021453	-0.097035	-0.074086	-0.049525		
7	0.16889	-0.027031	0.013115	-0.094654		
11	0.23336	0.30683	0.16310	-0.037955		
15	0.14967	-0.034828	0.22904	0.30244		

$$p = \left[ \frac{\omega \rho \left( \frac{d}{2} \right) \xi_o e^{-jkr}}{\sqrt{\xi_o^2 - 1} kr} \right] p_r(\theta),$$

$$p_r(\theta) = \sum_n (-j)^{-n} \frac{\left\{ \sum_i V_i e^{j\delta_i} I_i^{0n} \right\} S_{0n}(h, \cos \theta)}{N_{0n} \left[ \frac{d}{d\xi} R_{0n}^{(4)}(h, \xi) \right]_{\xi=\xi_o}} \quad (26)$$

TABLE 4  
Total Impedances for the Eight Active Zones

Zone	Self Impedance* $Z_{ii}$	Total Impedance*† $Z_i$
14	$0.22904 + j 0.30244$	$0.35212 + j 0.18316$
10	$0.23336 + j 0.30684$	$0.50739 + j 0.18450$
6	$0.24371 + j 0.30871$	$0.50999 + j 0.10721$
2	$0.24398 + j 0.30788$	$0.45398 + j 0.027494$
3	$0.24398 + j 0.30788$	$0.45397 + j 0.027498$
7	$0.24369 + j 0.30870$	$0.50996 + j 0.10720$
11	$0.23336 + j 0.30683$	$0.50737 + j 0.18450$
15	$0.22904 + j 0.30244$	$0.35211 + j 0.18316$

\*All impedances are expressed as fractional parts of  $\rho c A$  where  $A$  is the actual area of a zone.

†For equal zonal velocities.

TABLE 5  
Total Impedances for Two, Three,  
or Four Active Zones

Zones Present	$Z_j$	Total Impedance*	
		Real	Imaginary
14, 10	$Z_{14}$	0.39215	0.26448
	$Z_{10}$	0.38303	0.27201
14, 10, 6	$Z_{14}$	0.67517	0.25294
	$Z_{10}$	0.64571	0.33461
	$Z_6$	0.81657	0.44298
14, 10, 6, 2	$Z_{14}$	0.57462	0.26710
	$Z_{10}$	0.58739	0.30195
	$Z_6$	0.48569	0.26732
	$Z_2$	0.50048	0.26898

\*Impedances are expressed as fractional parts of  $\rho c A$ , where  $A$  is the actual area of a zone.

in which  $r, \theta$  are the spherical coordinates referred to the origin. Since we are interested only in relative magnitudes of total pressure ( $= p_r$ ) as a function of angle, we write

$$p \propto |p_r(\theta)|. \quad (27)$$

The beam pattern function  $K(\theta)$  in decibel notation is defined here as

$$K(\theta) = 20 \log |p_r|. \quad (28)$$

Equation (26) is quite involved, and we restricted ourselves for the purposes of this report to the simple case of equal velocities on all eight rings. The factor  $V_i e^{j\delta_i}$  was therefore omitted in all of our computations. The sum  $n$  was taken from 0 to 10. Figures 3a and 3b show plots of the angle spheroidal wave functions  $S_{0n}(h, \cos \theta)$  vs  $\cos \theta$  for  $h = 6.6$  which were used in the computation of Eq. (27). Figure 4a shows a far-field pressure pattern generated by all eight zones, the pattern drawn to linear scale. Figure 4 b shows the same pattern drawn to decibel scale. It was decided at this point to draw all subsequent beam patterns to decibel scale. Figure 5a shows the pattern generated by zone 14 alone. Figure 5b shows the patterns generated by two, three, or four zones located above the equator. Figure 6 shows the far-field pressure patterns generated by two zones above the equator plus one or two zones below the equator. Figure 7 shows the far-field pressure patterns due to three zones above the equator plus one, two, three, or four zones below the equator. Figure 8 shows the far-field pressure patterns due to four zones above the equator plus one, two, three, or four zones below the equator. Figure 9 shows the far-field pressure patterns due to an equatorially symmetrical arrangement of two, four, six, or eight zones.

## CONCLUSION

The numerical computation of the radiation impedance and radiation patterns of zonal transducers on a hard prolate spheroidal baffle is clearly a very involved task. Still remaining to be conquered is the precision calculation of radial spheroidal wave functions for  $\xi_0$  not much greater than unity. We plan to repeat this calculation with altered spheroid eccentricity on a digital computer of much larger memory. However, the results of the exercise represented by the above work are useful in their own right in that they represent our first efforts to understand the radiation impedance of zonal arrays on baffles of other than planar or spherical shape.

## ACKNOWLEDGMENT

The author expresses his gratitude to R. V. Baier and A. R. Stickley of the Transducer Branch, Sound Division, for valuable assistance in the preparation and checking of the various digital computer programs used in the numerical calculations of this report.

## REFERENCES

1. Flammer, C., "Spheroidal Wave Functions," Stanford Univ. Press, Stanford, Calif., 1957
2. Stratton, J.A., Morse, P.M., *et al.*, "Spheroidal Wave Functions," New York:Wiley, 1956
3. Morse, P.M., and Feshbach, H., "Methods of Theoretical Physics," New York:McGraw-Hill, 1953
4. Robey, D.H., "On the Radiation Impedance of an Array of Finite Cylinders," *J. Acoust. Soc. Amer.* **27**:706 (errata 1227) (1955)

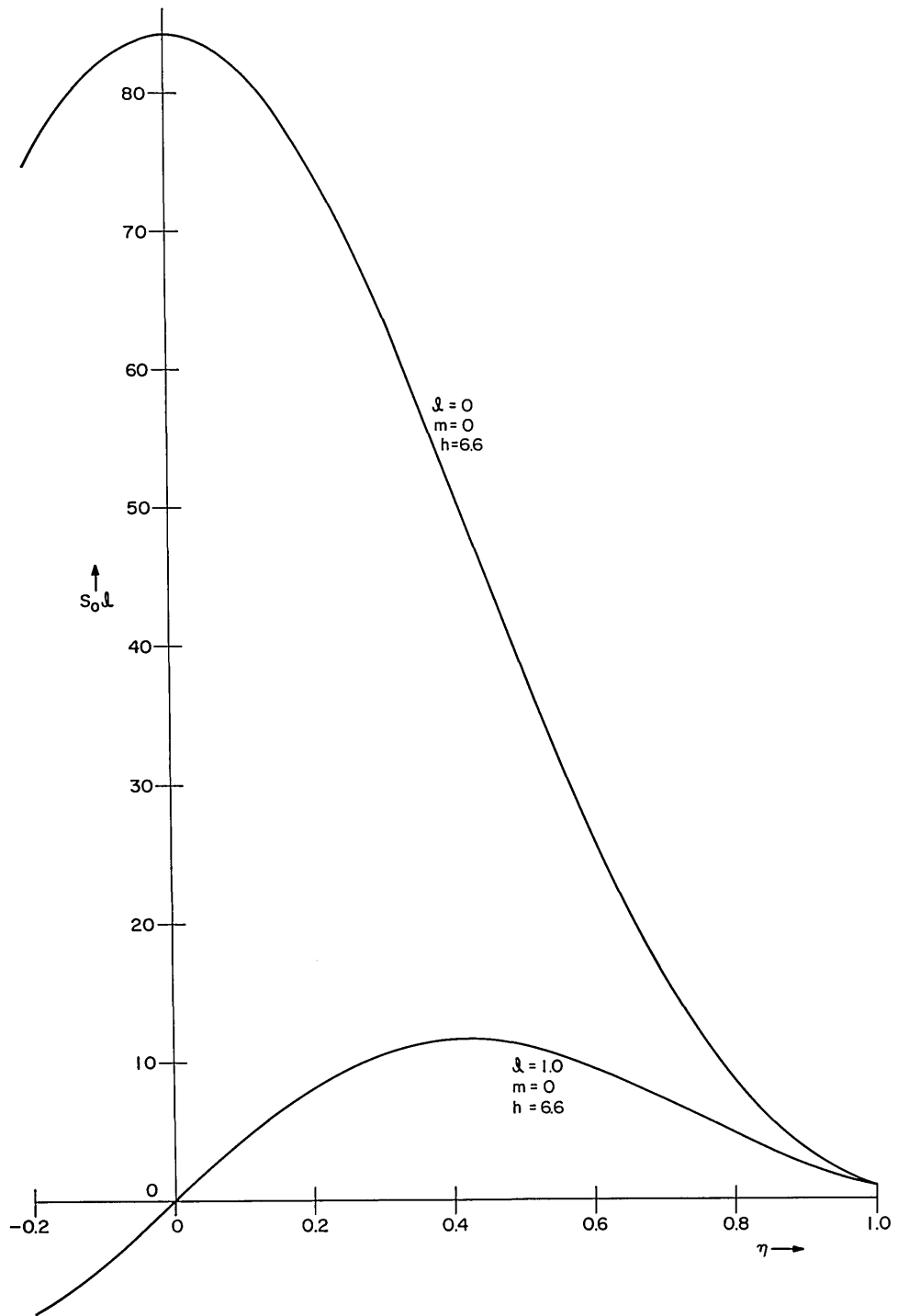


Fig. 3a — Angle spheroidal wave functions  $S_{0n}(b, b, \eta)$  versus  $\eta$  for  $n = 0, 1$

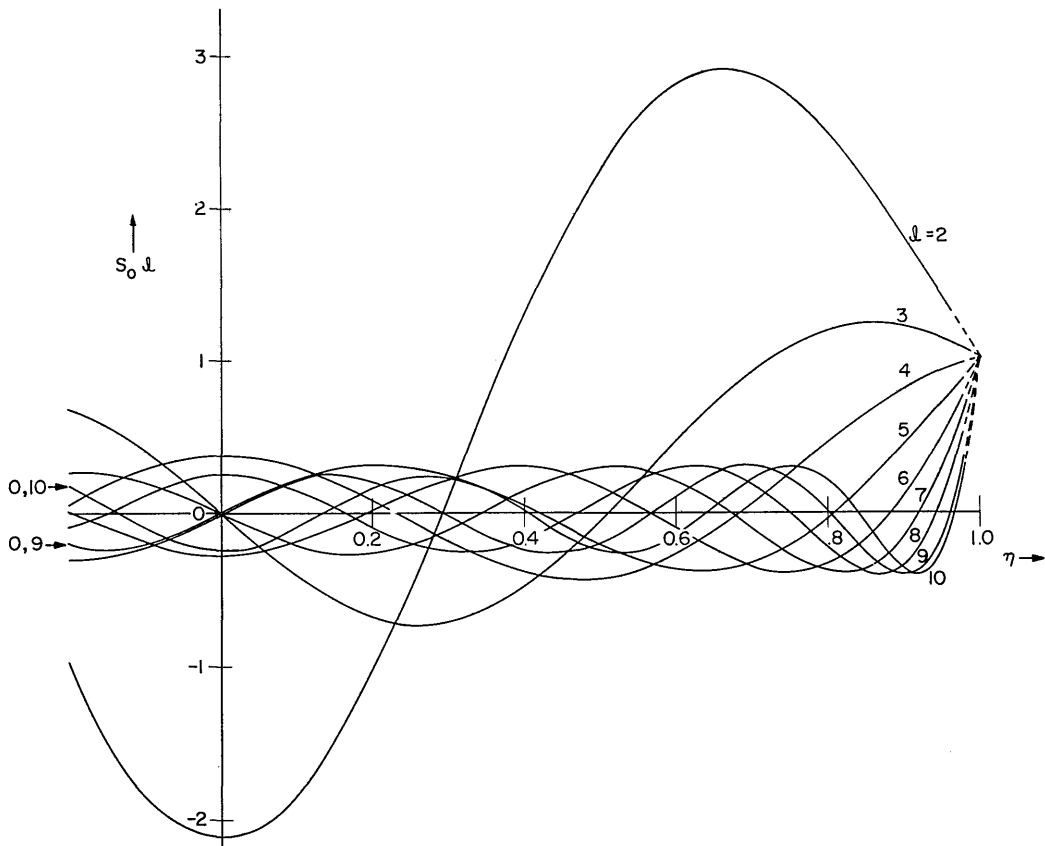


Fig. 3b — Angle spheroidal wave functions  $S_{0n}(b, b, \eta)$  versus  $\eta$  for  $n = 2, 3, \dots, 10$

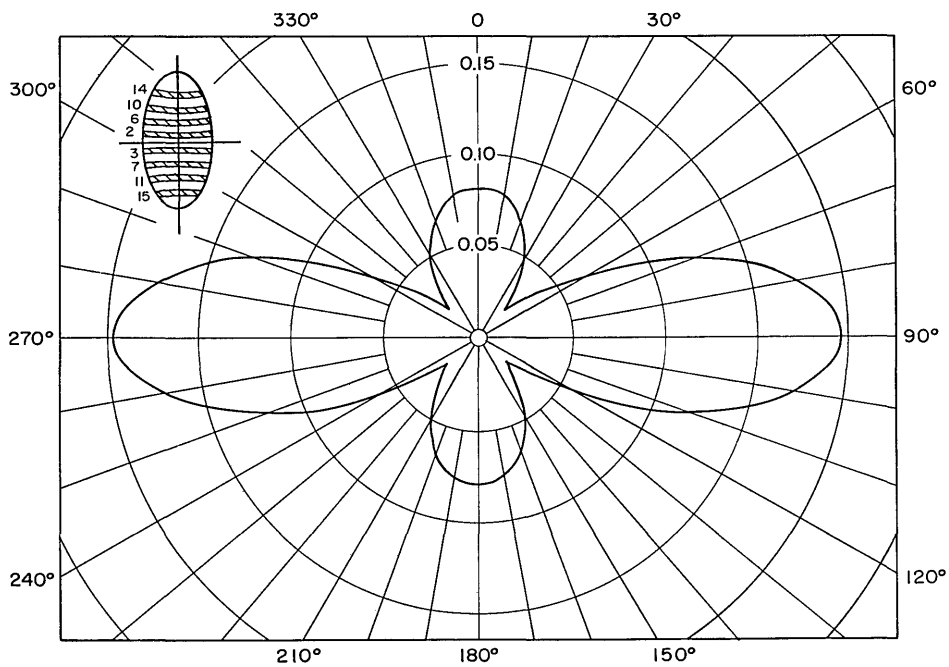


Fig. 4a — Far-field pressure pattern on a linear scale for eight zones moving with equal velocities

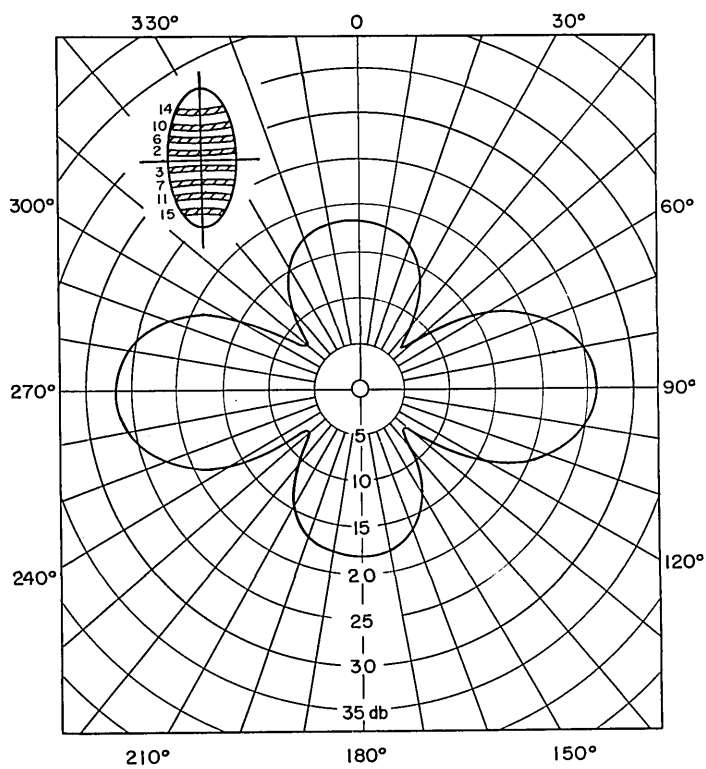


Fig. 4b — Far-field pressure pattern on a logarithmic scale for eight zones moving with equal velocities

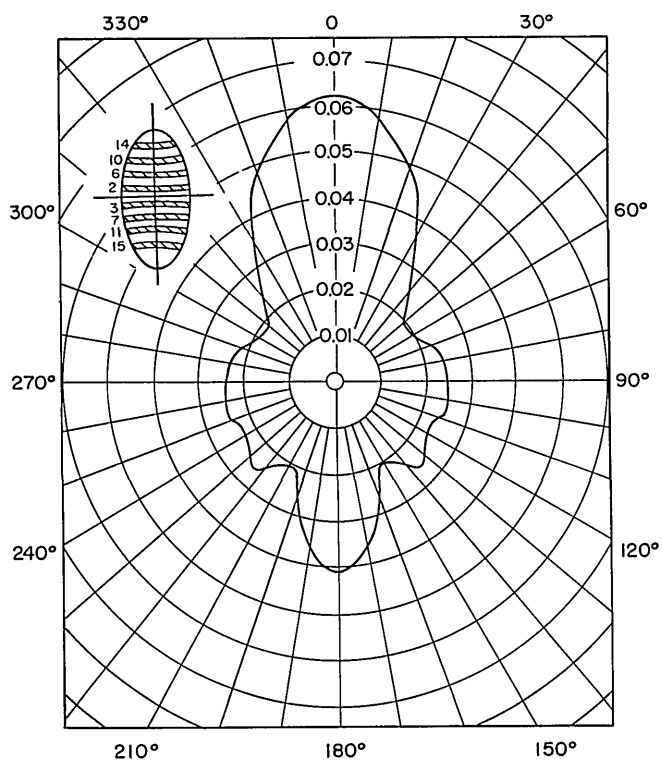


Fig. 5a — Far-field pressure pattern due to zone 14 with no other zones present

Fig. 5b — Far-field pressure patterns due to two, three, and four zones above the equator, all moving with equal velocities

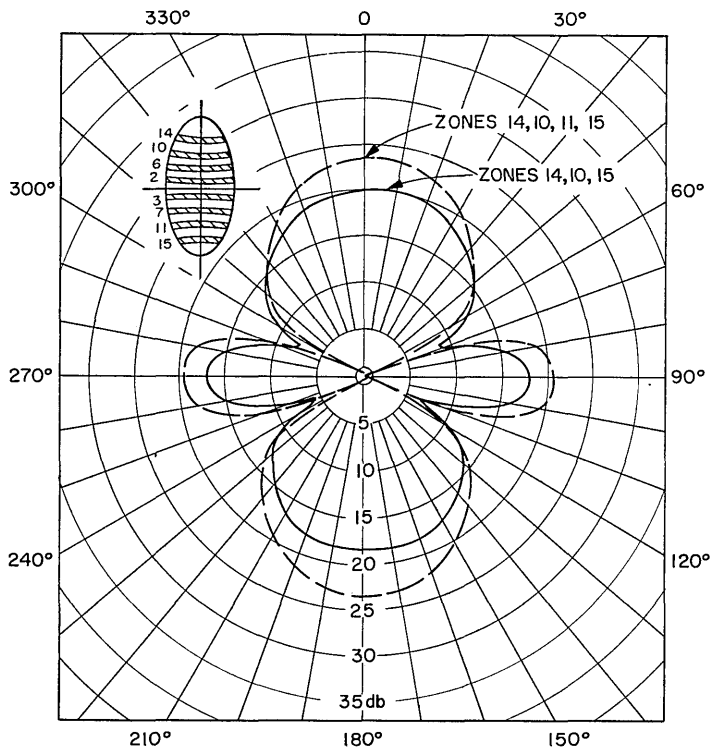
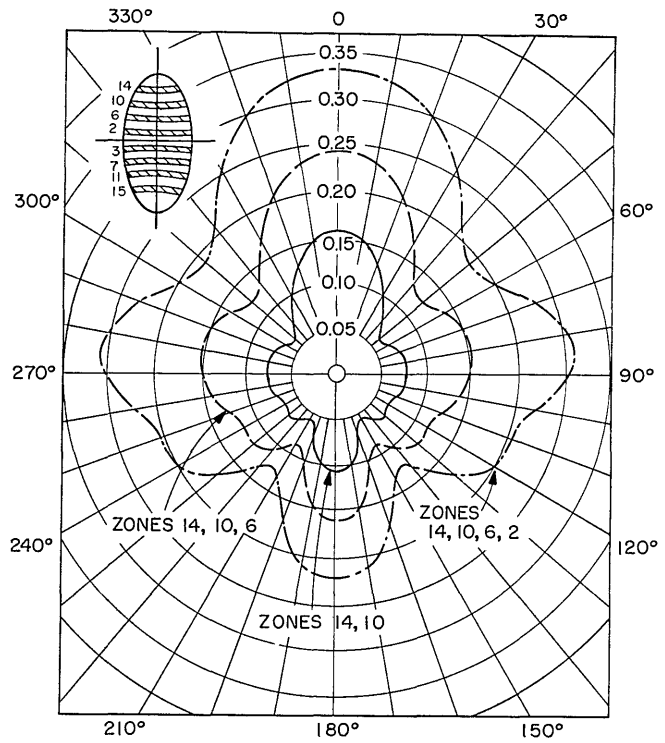


Fig. 6 — Far-field pressure patterns due to two zones above the equator plus one or two zones below the equator, all moving with equal velocities

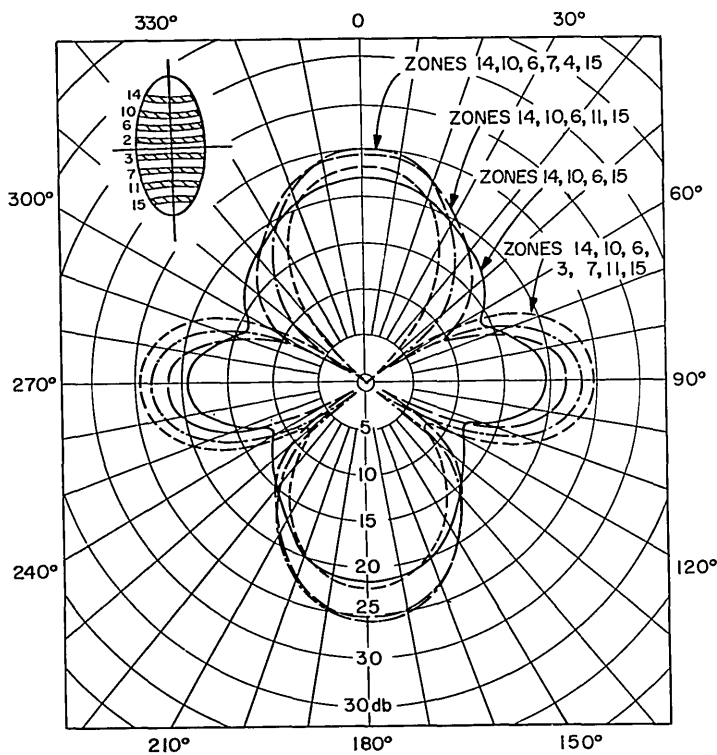


Fig. 7 - Far-field pressure patterns due to three zones above the equator plus one, two, three, or four zones below the equator, all moving with equal velocities

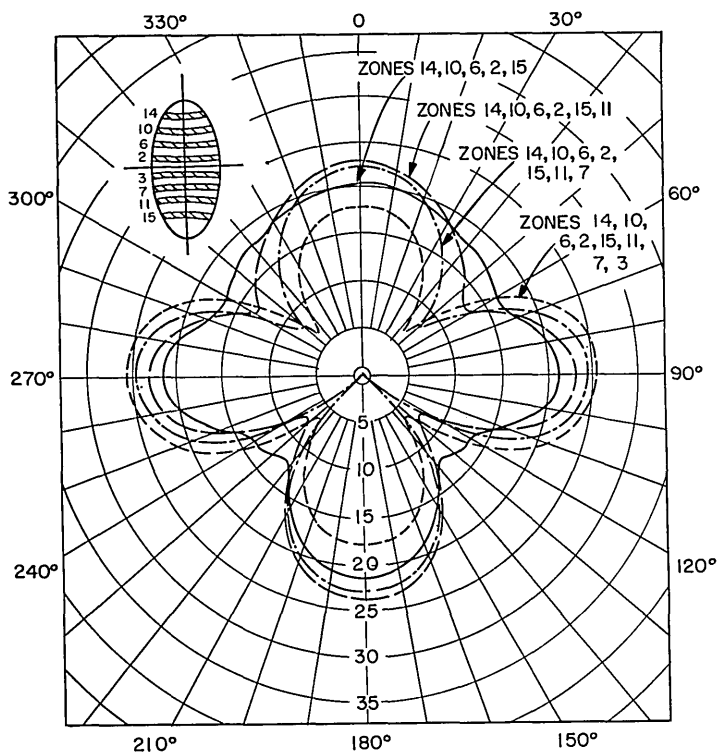


Fig. 8 - Far-field pressure patterns due to four zones above the equator plus one, two, three, or four zones below the equator, all moving with equal velocities

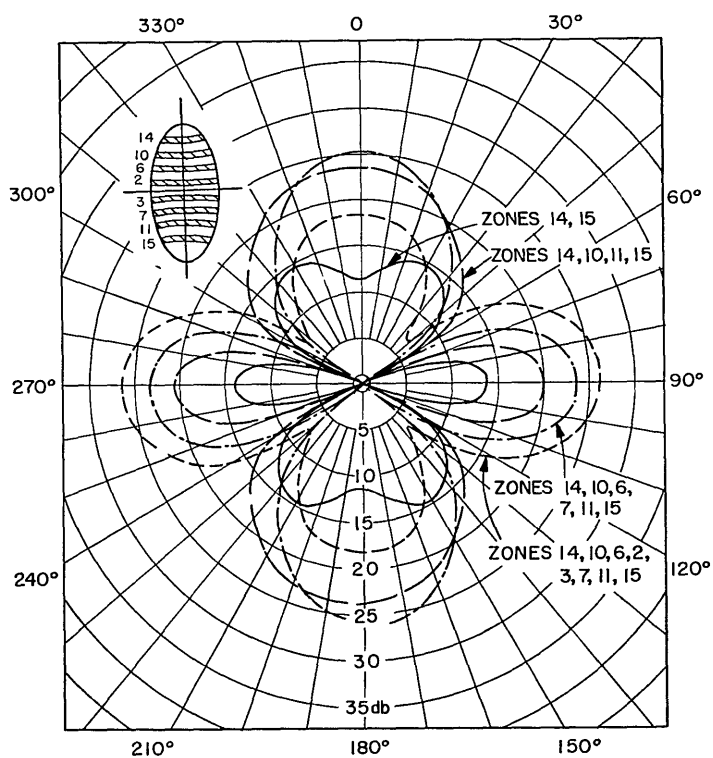


Fig. 9 — Far-field pressure patterns due to two, four, six, or eight equatorially symmetrical zones, all moving with equal velocities